

Comparing early to middle Miocene terrestrial climate simulations with geological data

N. Herold^{1,*}, R.D. Müller¹, and M. Seton¹

¹EarthByte Group, School of Geosciences, University of Sydney, Sydney, NSW 2006, Australia

ABSTRACT

The early to middle Miocene was significantly warmer than present, particularly at high latitudes. Relatively few climatic details are known about this time period compared with earlier (e.g., Cretaceous/Eocene) and later (e.g., Quaternary) intervals. In this study terrestrial proxy data are quantitatively compared with three simulations of early to middle Miocene climate (20–14 Ma) carried out using the National Center for Atmospheric Research (NCAR) Community Atmosphere Model 3.1 (CAM) and Community Land Model 3.0 (CLM). Three different meridional sea-surface temperature gradients are prescribed in order to test a range of plausible climates. Our simulations yield generally cooler and more arid conditions than indicated by the proxy record. Mean model-data discrepancies for precipitation and temperature decrease from –320 to –170 mm/yr and –0.5 to –0.4 °C, respectively, when tropical sea-surface temperatures are increased by ~4 °C from inferred Miocene values to near modern values. The poor agreement with respect to mean annual precipitation may be attributed to the preclusion of an interactive ocean model and/or model bias.

INTRODUCTION

Numerical simulations of Earth's past climate are often compared with the proxy record in order to determine the accuracy of the model solution. Despite the typically large uncertainties associated with the reconstruction of boundary conditions, model formulation, and derivation of proxy data, this remains the only measure of a model's ability to accurately reproduce climates different to that of the pres-

ent. Of these, the largest source of uncertainty arguably arises from model boundary conditions, where values for large areas of the globe are predicted or interpolated from relatively few data points (e.g., for vegetation or sea-surface temperature [SST]).

In atmosphere only General Circulation Models (GCMs), SST is the most influential boundary condition on the simulated climate, as oceanic responses to the atmosphere are precluded. Over the past decade, increasing evidence of diagenesis in low latitude fossils of planktonic foraminifera have revealed a significant cold bias in $\delta^{18}\text{O}$ derived temperatures (Pearson et al., 2001; Williams et al., 2005). This has called into question previous SST reconstructions (e.g., O'Connell et al., 1996; Sloan and Thomas, 1998). Sensitivity studies show that atmospheric and implied surface ocean characteristics can differ dramatically with varying low and/or high latitude SSTs (Huber and Sloan, 2000; Rind, 2000). Therefore, as a second-order indication of accuracy, it is useful to constrain reconstructed SSTs by comparing the terrestrial climate they force in a model with the proxy record (e.g., Lunt et al., 2008a; Sloan and Barron, 1992). However, such a method assumes proxy data are accurate to within the degree of error of climate models, and representative of the grid cells they occupy in model space (discussed later).

Here we focus on three simulations of early to middle Miocene climate, a period of distinct global warming terminated by abrupt cooling in the late-middle Miocene. Each simulation is forced with a different meridional SST gradient based on plausible variations to published $\delta^{18}\text{O}$ and Mg/Ca data. To determine the meridional SST gradient that best matches terrestrial proxy data we compare model-data discrepancies between simulations. We subsequently discuss uncertainties in our results and draw comparisons with other studies of Miocene climate.

EXPERIMENT DESIGN

Simulations are conducted using the National Center for Atmospheric Research (NCAR) Community Atmosphere Model 3.1 (CAM; Collins et al., 2006) and Community Land Model 3.0 (CLM; Vertenstein et al., 2004). Both CAM and CLM are configured for T31 resolution, representing 3.75° in longitude and ~3.75° in latitude. CAM uses a hybrid sigma-pressure vertical coordinate system with 26 levels. CLM simulates temperature and water variables for ten layers of soil and up to five layers of snow. Each land grid cell is prescribed up to four out of an available 15 vegetation types, constituting a biome. Each vegetation type differs in albedo, root distribution, aerodynamic, and photosynthetic parameters. CAM and CLM reproduce modern-day climate reasonably well and coupled to the NCAR ocean and sea-ice models, have been used to simulate deep-time paleoclimate intervals (e.g., Kiehl and Shields, 2005). However, despite improvements over earlier versions, several biases remain in the models, including underestimation of implied ocean heat transport, excessive Northern Hemisphere low cloud production, and anomalous continental precipitation (Collins et al., 2006; Dickinson et al., 2006).

This study analyzes results from three simulations forced with newly constructed boundary conditions. Inherently, a trade-off exists between the spatial and temporal resolution of proxy data and the limited information available for the Miocene makes a longer time interval favorable. Therefore published information primarily for the late-early to early-middle Miocene are utilized to reconstruct vegetation and SSTs (ca. 20–14 Ma).

Each simulation differs only in regard to SST distribution. Twelve months of zonally varying SSTs are prescribed in each simulation to replace a mixed-layer ocean model supported

*nicholas.herold@sydney.edu.au

by CAM. While prescribing SSTs precludes important feedbacks between the ocean and atmosphere we consider it more useful than applying a mixed layer ocean model to approximate Miocene conditions. At the peak of Miocene warming, deep water and polar SSTs were more than 5 °C warmer than present (Lear et al., 2000), implying that sea ice could only be seasonal. Such conditions have proven difficult to reproduce using mixed layer or coupled ocean models even when applying higher greenhouse gas concentrations (e.g., Huber and Sloan, 2001; Steppuhn et al., 2007).

Our first simulation is forced with SSTs based solely on published proxy data (referred to as P-MIO). A Gaussian curve is fitted to proxy data using the least-squares method (Fig. 1). These values are extended zonally to produce a global mean annual SST data set. Monthly zonal SSTs are calculated based on modern-day seasonality. At each latitude, modern-day zonal mean SST for each month is subtracted from the modern-day annual zonal mean from the same latitude; these differences are then applied to the Miocene data set to construct 12 months of zonally uniform SSTs. To account for reduced

seasonality during warmer climates—due to ice-albedo feedbacks—the magnitude of these differences is reduced by 30% (after O’Connell et al., 1996). Finally, the east-west SST gradient from each modern-day month is applied to each respective Miocene month. Although modern-day east-west gradients may not be representative of Miocene surface conditions, zonally constant SSTs may result in larger model-data discrepancies (Sloan et al., 2001). Furthermore, the similarities between Miocene and modern-day geography, along with partial reconstructions of Miocene surface currents (Kennett et al., 1985; Wright and Thunell, 1988), imply large-scale surface conditions, such as boundary currents, were similar to the modern. Therefore, we believe modern-day east-west gradients provide a closer approximation to Miocene SSTs than zonally constant values. Sea ice is assumed to be absent in both hemispheres given minimum SSTs are above freezing.

To examine the validity of reconstructing SSTs based solely on proxy data, we test two sources of uncertainty in P-MIO: (1) the limited number of data points used to constrain the mean annual meridional SST gradient (Fig. 1),

and (2) the extent to which proxy SST estimates are preserved in the final reconstruction. Using modern-day SSTs from CAM we calculate mean annual values at locations where Miocene proxy data exist (Fig. 1 caption; using modern-day longitudes and latitudes). Using the least-squares method, a Gaussian curve is fitted to these values to reconstruct zonal mean SSTs, as is done for P-MIO (Fig. 2). A minimum value of -1.8 °C is applied (the freezing point of seawater). The mean absolute difference between the reconstructed meridional SST gradient and a zonal mean of the modern-day CAM SST distribution is 0.9 °C. Therefore, given a limited number of accurate SSTs we propose it is possible to reconstruct an approximate meridional temperature gradient for a given time period. However, we note the current margin of error for proxy data, particularly at low latitudes, does not allow a high degree of accuracy for this kind of reconstruction (Crowley and Zachos, 2000).

To determine the extent to which proxy SSTs are preserved in P-MIO we perform a site comparison (Fig. 3). The absolute mean difference between proxy SSTs and the corresponding values in P-MIO is 3.5 °C. This is largely attributed to the variation in proxy SSTs around the reconstructed meridional gradient (Fig. 1). Assuming magnitudes of east-west temperature variation were similar in the Miocene as they are today, the range of proxy SSTs around the reconstructed meridional gradient should be up to an order of magnitude smaller (c.f. Figures 1 and 2). Nonetheless, the mean difference between proxy SSTs and P-MIO is within the error predicted for pre-Pleistocene $\delta^{18}\text{O}$ derived SSTs (Crowley and Zachos, 2000).

P-MIO is characteristic of the low meridional SST gradients traditionally inferred for past warm climates (e.g., Sloan and Thomas, 1998). The implied ocean heat transport required to maintain this temperature gradient is significantly higher than modern and arguably unrealistic (Fig. 4). Given the increasing evidence of diagenetic alteration of low latitude carbonate samples (Pearson et al., 2001; Pearson et al., 2007; Williams et al., 2005) and the inability of coupled models to simulate the ocean heat transport required to lower meridional temperature gradients sufficiently (e.g., Huber and Sloan, 2001), such a low gradient is unlikely to have existed. To test the effects of altered meridional gradients on model-data discrepancies two additional simulations are performed based on P-MIO. Our second SST distribution represents a temperate Miocene climate (T-MIO) and is created using the same method as P-MIO except with peak tropical SSTs fixed at ~ 28 °C before a curve of best fit is calculated. This distribution

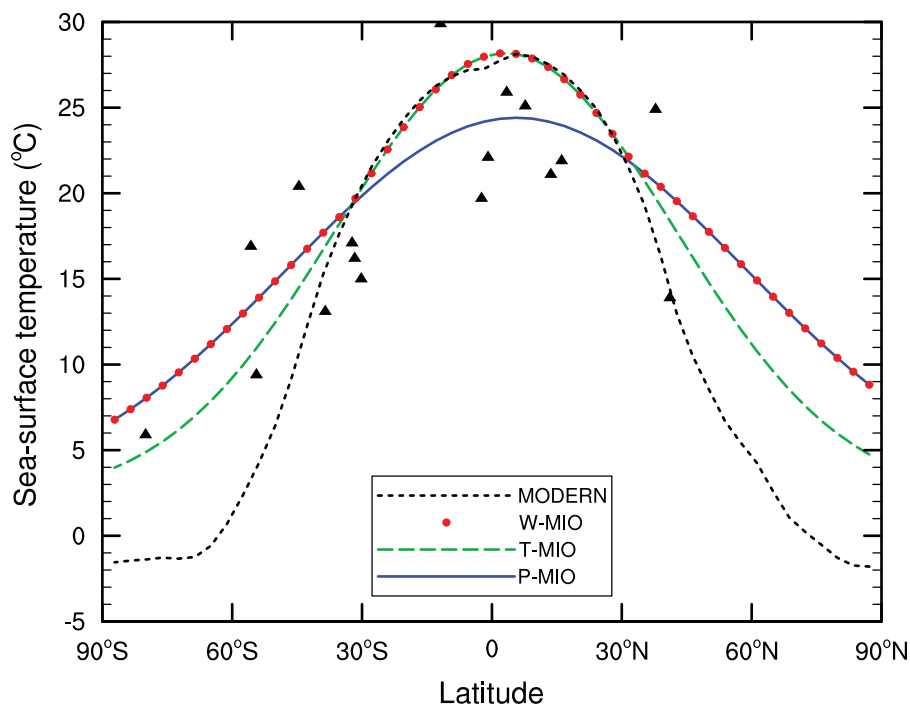


Figure 1. Meridional gradients used to derive global SST distributions for each simulation (see text for details) as well as modern-day mean annual zonal SST (dotted line). Miocene proxy data (triangles) from Devereux (1967), Pagani et al. (1999a), Savin et al. (1975), Shackleton and Kennett (1975), Shevenell et al. (2004), Stewart et al. (2004), and Van der Smissen et al. (1996). A SST of 6 °C is applied for 80°S based on bottom water temperatures from Lear et al. (2000) and assuming bottom water formation occurred at high latitudes (Sykes et al., 1998).

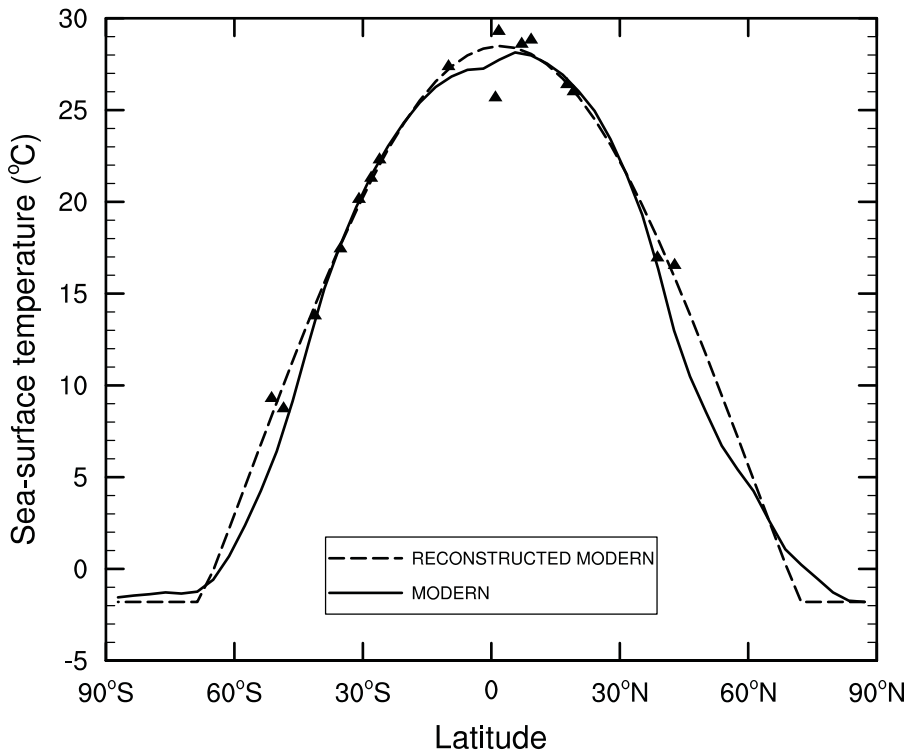


Figure 2. Modern-day meridional SST gradient (dashed line) reconstructed from mean annual SSTs at proxy data locations (filled triangles) and annual zonal mean of modern-day SST (solid line; see text for details).

tests the assumption that estimates of tropical SST are biased toward cooler values and are in reality closer to the modern day. Consequently, while tropical SSTs are increased, middle to high latitude SSTs are decreased relative to P-MIO (Fig. 1). The third distribution represents a warm estimate of Miocene climate (W-MIO) and is based on P-MIO except with low latitude SSTs (within 30° of the equator) smoothed to those calculated for T-MIO (Fig. 1). As in T-MIO, our third distribution tests the assumption that tropical SSTs were close to the modern day but that extra-tropical SSTs corresponded to those in P-MIO. The implied ocean heat transports in T-MIO and W-MIO fall closer toward modern-day values than P-MIO though still vary by greater than 1 PW at some latitudes (Fig. 4) and are larger than that calculated by a coupled model of Miocene climate (von der Heydt and Dijkstra, 2006).

Miocene vegetation is based on Wolfe (1985) with amendments from subsequent studies (Fig. 5). Most notable is the addition of a moderate size East Antarctic ice sheet (Lear et al., 2000; Pekar and DeConto, 2006); however, West Antarctica and Greenland remain ice free. Other distinguishing features of Miocene vegetation, compared with the modern, are the greater poleward expanse of tropical

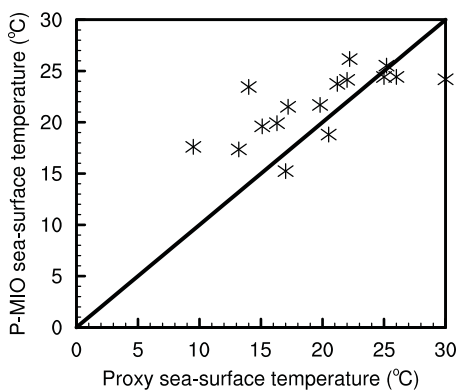


Figure 3. Discrepancy between proxy estimates of SST and P-MIO (see text for details).

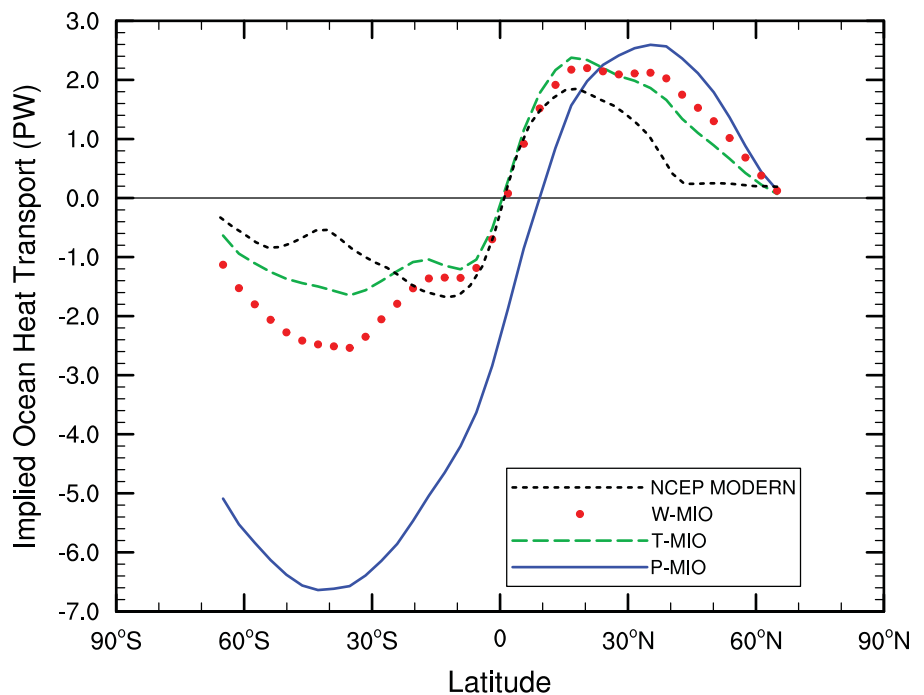


Figure 4. Implied ocean heat transport calculated for each simulation and modern-day ocean heat transport (short dashed line).

vegetation as well as the absence of middle latitude deserts (e.g., the Sahara). We classify our vegetation types to a set of biomes modified from Bonan et al. (2002) (Fig. 5). These modifications include replacing C_4 grass with C_3 grass, since the former did not become widespread until the late Miocene (Pagani et al., 1999b), and creating a temperate broadleaf evergreen biome to more accurately represent Wolfe's (1985) middle latitude vegetation (c.f. Wolfe, 1985; Bonan et al., 2002).

Miocene geography and topography are based on the rotations of a plate kinematic model and published paleoelevation and paleogeographic data (Herold et al., 2008). While the magnitude of uplift of the Tibetan Plateau since the middle Miocene is controversial (Harris, 2006), it is assumed that the plateau had achieved a near modern elevation of 4700 m. The northern, central, and southern Andes are reduced from their modern elevations to 500, 1000, and 600 m, respectively. For further details see Herold et al. (2008).

The majority of published Miocene CO_2 concentrations range from 300 to 400 ppmv (Ber-

ner and Kothavala, 2001; Cerling, 1991; Francois et al., 2005; Pearson and Palmer, 2000; Royer et al., 2001), though there is some support for higher (Kürschner et al., 2008; Retallack, 2001; Sheldon, 2006) and lower (Pagani et al., 1999a) concentrations. We therefore prescribe a 1990 concentration of 355 ppmv. CH_4 and N_2O are set to pre-industrial values (760 and 270 ppb, respectively). Obliquity, eccentricity and longitude of moving vernal equinox are set to 1950 values. The prescribed solar constant is 1365 W/m^2 . For each simulation, the past 30 yr of a 70 yr integration are averaged to form model climatologies.

MODEL-DATA COMPARISON

Methods

Mean annual 2 m air temperature and mean annual precipitation from each simulation are compared with terrestrial proxy data from the late-early to early-middle Miocene (ca. 20–14 Ma; Tables 1 and 2). The majority of proxy data are based on modern-day analogs of

fossil flora (the coexistence approach; Mosbrugger and Utescher, 1997) or physiognomic analysis (Climate-Leaf Analysis Multivariate Program; Wolfe, 1993). Other estimates are derived from paleosols and fossil fauna. 2 m air temperature is used for comparison as it provides a closer approximation to canopy temperatures (Sloan and Rea, 1996).

Climatic Variability and Error

Prior to comparing proxy data and model output, error margins for each are defined. Error margins for proxy data are taken from their respective studies, however, where no values are provided conservative errors of $\pm 1 \text{ }^\circ\text{C}$ and $\pm 100 \text{ mm/yr}$ are applied for temperature and precipitation, respectively.

To account for climatic variability in each simulation we establish upper and lower bounds of mean annual 2 m air temperature and mean annual precipitation for each location, defined by the maximum and minimum mean annual values calculated over the 30 years used for analysis (after Steppuhn et al., 2007). Accounting

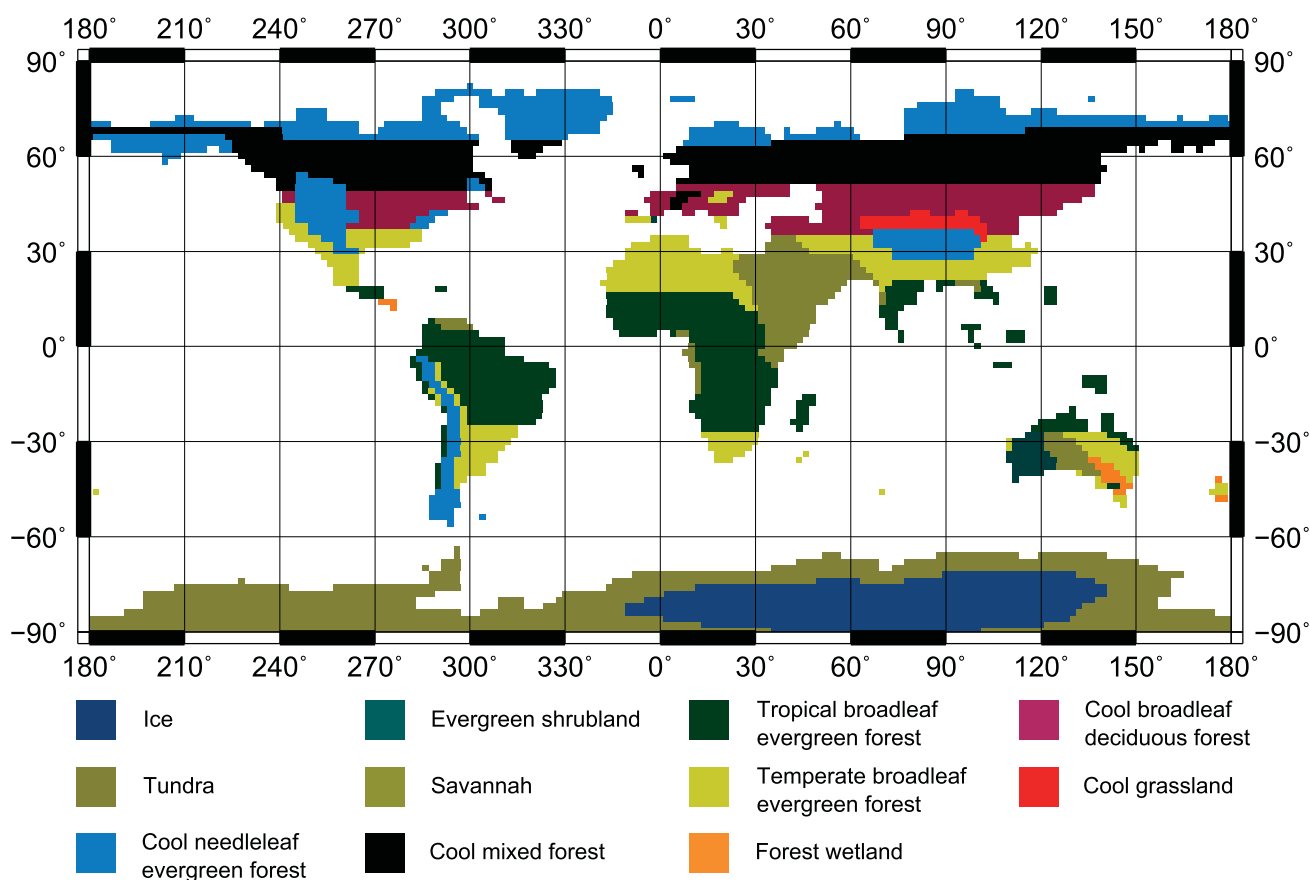


Figure 5. Reconstructed Miocene vegetation based on Wolfe (1985) with amendments from published data (Bialkowski et al., 2006; Christophel and Greenwood, 1989; Ducrocq et al., 1994; Graham, 1987; Ivanov et al., 2002; Jacobs, 2004; Kemp, 1978; Lear et al., 2000; Martin, 1990; Martin, 2006; Mildenhall, 1980; Pekar and DeConto, 2006; Sluiter et al., 1995; Wynn and Retallack, 2001).

TABLE 1. COMPARISON OF LOWER AND UPPER LIMITS OF MEAN ANNUAL TEMPERATURE (MAT) FROM PROXY DATA AND EACH SIMULATION

Location	Paleo long/lat*	Topo error (°C) [†]	Proxy MAT (°C) [§]		P-MIO-Proxy MAT (with topographic correction) (°C)	T-MIO-Proxy MAT (with topographic correction) (°C)	W-MIO-Proxy MAT (with topographic correction) (°C)	Ref.#
			Lower	Higher				
Weisselster and Lausitz Basin, NE Germany	7/52	1.95	17	19	0.0 (0.0)	-2.7 (-0.7)	0.0 (0.0)	1
Lower Rhine Embayment, NW Germany	7/52	1.95	15.5	21	0.0 (0.0)	-1.2 (0.0)	0.0 (0.0)	2
Schrotzberg, Southern Germany	6/47	1.95	15	16	0.0 (0.0)	-1.2 (0.0)	0.0 (0.0)	3
NW Bulgaria	21/42	1.95	16	18	1.5 (0.0)	0.4 (0.0)	0.4 (0.0)	4
Lower Rhine Embayment, NW Germany	7/52	1.95	15.7	16.2	0.0 (0.0)	-1.4 (0.0)	0.0 (0.0)	5
Schrotzberg, Southern Germany	6/47	1.95	14.4	16.5	0.0 (0.0)	-0.6 (0.0)	0.0 (0.0)	6
Kovago-old al	17/47	1.95	15	22.3	0.0 (0.0)	-0.8 (0.0)	0.0 (0.0)	7
Southern Germany (see ref. for locations)	8.9/47.3	0.53	17.4	20.5	0.0 (0.0)	-3.6 (-3.1)	-0.2 (0.0)	8
Ukraine	20.5/47.6	7.07	15.6	18.4	0.0 (0.0)	-1.4 (0.0)	0.0 (0.0)	9
Bigadic, Turkey	25.1/38.3	1.85	17.2	21.3	0.0 (0.0)	0.0 (0.0)	0.0 (0.0)	10
Samsun-Havza, Turkey	33.3/40	2.63	17.2	20.8	0.0 (0.0)	0.0 (0.0)	0.0 (0.0)	10
Pannonian Basin	18.5/44.55	1.95	14.1	16.4	2.2 (0.2)	0.0 (0.0)	1.0 (0.0)	11
Popovac, Serbia	18.3/42.9	0.41	14.4	21.3	0.0 (0.0)	0.0 (0.0)	0.0 (0.0)	12
Latrobe Valley, SE Australia	146/-45	1.95	18	20	-3.7 (-1.7)	-5.3 (-3.3)	-4.1 (0.0)	13
Gippsland Basin, SE Australia	144/-45	0.71	12	14	0.0 (0.0)	0.0 (0.0)	0.0 (0.0)	14
Gippsland Basin, SE Australia	146/-45	1.95	13	18	0.0 (0.0)	-0.3 (0.0)	0.0 (0.0)	15
Kangaroo Well, Central Australia	129.7/-29.7	1.80	14	20	0.0 (0.0)	0.8 (0.0)	0.0 (0.0)	16
Yunnan Province, SW China	95/22	1.95	18.8	20.5	0.0 (0.0)	2.0 (0.0)	2.8 (0.9)	17
Shanwang, China	116.5/38.5	1.30	15.3	17.2	-1.6 (-0.3)	-3.1 (-1.8)	-2.5 (-1.2)	18
Shanwang, China	116.5/38.5	0.86	10.9	14.5	0.0 (0.0)	0.0 (0.0)	0.0 (0.0)	19
Shanwang, China	116.5/38.5	1.30	9.5	11.2	0.5 (0.0)	0.0 (0.0)	0.0 (0.0)	20
Naming Basin, Southern Tibet	86.9/30.8	7.31	3.4	10.2	-8.1 (-0.8)	-4.3 (0.0)	-4.5 (0.0)	21
Picture Gorge Subgroup, N. America	-114.7/44.8	3.06	8	16	0.0 (0.0)	0.0 (0.0)	0.0 (0.0)	22
Eastern Oregon, N. America	246/45	1.95	7.7	17.7	0.0 (0.0)	0.0 (0.0)	0.0 (0.0)	23
Alaska, N. America	-135.6/69	1.35	8	10	-1.7 (-0.3)	-3.8 (-2.5)	-1.5 (-0.1)	24
Cape Blanco, N. America	-116.25/45	0.65	15.6	17.6	-0.8 (-0.2)	-4.0 (-3.4)	-2.7 (-2.1)	25
Waeaverville, N. America	-116.25/43	0.65	15.2	17.2	0.0 (0.0)	-2.2 (-1.4)	-0.7 (0.0)	25
Cook Inlet, N. America	-147/62	1.32	10.2	23.8	0.0 (0.0)	0.0 (0.0)	0.0 (0.0)	26
Potosi, Bolivia	-62.8/-21.7	11.90	19.4	23.8	0.0 (0.0)	1.7 (0.0)	1.3 (0.0)	27
Feje, Ethiopia	33.6/2.3	1.47	23.5	28.5	-2.4 (-0.9)	0.0 (0.0)	0.0 (0.0)	28
			Mean:		-0.5 (-0.1)	-1.1 (0.5)	-0.4 (-0.2)	

Note: Model-data discrepancies in columns 6–8 represent differences between ranges of proxy MATs (columns 4 and 5) and model-predicted MATs (not shown). Values in brackets factor in topographic error (column 3). A zero value indicates overlap. All proxy data are derived from fossil flora except references 16, 22, 23, and 28.

[†]Where paleolatitudes and longitudes are not provided, values are calculated using modern coordinates, a plate kinematic model, and the rotations of Müller et al. (2008).

[‡]Where precise latitudes and longitudes of proxy locations are not provided, we assume a topographic error of 300 m = ±1.95 °C (taken from the mean of all other proxy locations).

[§]Where no error margin is provided in the literature, an error of ±1 °C is applied (shown in bold).

[¶]References: 1—Mosbrugger et al. (2005); 2—Utescher et al. (2000); 3—Uhl et al. (2006); 4—Ivanov et al. (2002); 5—Mosbrugger and Utescher (1997); 6—Uhl et al. (2003); 7—Uhl et al. (2007); 8—Bohme et al. (2007); 9—Syabryaj et al. (2007); 10—Akgun et al. (2007); 11—Erdei et al. (2007); 12—Utescher et al. (2007); 13—Sluiter et al. (1995); 14—Greenwood (1994); 15—Kemp (1978); 16—Meghian et al. (2004); 17—Zhao et al. (2004); 18—Liang et al. (2003); 19—Yang et al. (2007); 20—Sun et al. (2002); 21—Spicer et al. (2003); 22—Sheldon (2006); 23—Retallack (2004); 24—White and Ager (1994); 25—Wolfe (1994b); 26—Wolfe (1994a); 27—Gregory-Wodzicki et al. (1998); 28—Wiemann et al. (1999).

TABLE 2. COMPARISON OF LOWER AND UPPER LIMITS OF MEAN ANNUAL PRECIPITATION (MAP) FROM PROXY DATA AND EACH SIMULATION

Location	Paleo long/lat*	Proxy MAP (mm) [†]		Model-Proxy MAP (mm/yr)			Ref. [§]
		Lower	Higher	P-MIO	T-MIO	W-MIO	
Lower Rhine Embayment, NW Germany	7/52	1250	1450	-674	-302	-584	2
Schrotzberg, Southern Germany	6/47	1200	1400	-410	0	0	3
NW Bulgaria	21/42	1100	1300	-486	-57	-123	4
Lower Rhine Embayment, NW Germany	7/52	1231	1355	-655	-283	-565	5
Southern Germany	8.9/47.3	931	1360	-141	0	0	8
Ukraine	20.5/47.6	1122	1213	0	0	0	9
Bigadic, Turkey	25.1/38.3	1217	1322	-642	-539	-412	10
Samsun-Havza, Turkey	33.3/40	1217	1322	-265	-339	-453	10
Pannonian	18.5/44.55	916	1232	-341	-21	0	11
Popovac, Serbia	18.3/42.9	1255	1613	-680	-360	-334	12
Latrobe Valley, Australia	146/-45	1600	1800	-531	-222	-189	13
Gippsland Basin, Australia	146/-45	1400	1600	-331	-22	0	15
Kangaroo Well, Australia	129.7/-29.7	300	600	0	0	0	16
Yunnan Province, Mangdan coal mine, SW China	95/22	1170	1300	183	0	0	17
Shanwang, China	116.5/38.5	996	1281	-148	0	0	18
Shanwang, China	116.5/38.5	1107.3	1880	-260	0	0	19
Columbia River, Picture Gorge Subgroup	-114.7/44.8	500	900	0	0	0	22
Eastern Oregon	-114/45	604	1098	0	0	0	23
			Mean:	-319	-129	-171	

Note: Model-data discrepancies in columns 5–7 represent differences between ranges of proxy MAP (columns 3 and 4) and model-predicted MAP (not shown). Zero indicates overlap. All proxy data are derived from fossil flora except references 16, 22, and 23.

*Where paleolatitudes and longitudes are not provided, values are calculated using modern coordinates, a plate kinematic model, and the rotations of Müller et al. (2008).

[†]Where no error margin is provided in the literature, an error of ± 100 mm/yr is applied (shown in bold).

[§]References as in Table 1.

for error in climate simulations is more challenging. The most common source of error in studies utilizing global models relates to differences in spatial scale between the model and proxy data. While the terrestrial proxy record may reflect extremely localized conditions, such as from a valley or wetland, each grid cell in our model represents up to 405 km². This results in smoother model topography and consequently inaccurate elevations at proxy sites; this is particularly significant in topographically complex regions such as the Tibetan Plateau and Andean Cordillera. We calculate error due to topographic uncertainty based on Sloan et al. (2001). For each proxy location we compare the modern-day elevation between a high-resolution topography (5 km \times 5 km) and a model generated topography (3.75° \times ~3.75°). The global mean lapse rate (-6.5 °C/km) is then applied to these differences to produce a model error margin for temperature at each location (Table 1).

Where simulated ranges of temperature or precipitation do not overlap with proxy values we consider model results too cool/warm or too wet/dry, otherwise we consider model and proxy data to agree (Tables 1 and 2). As summing model error margins and ranges of climatic variability would lead to a spurious comparison, we compare only the climatic variability of each simulation to proxy data and consider model error margins separately.

Mean Annual 2 m Air Temperature

In this section we compare simulated 2 m air temperature with proxy data. The mean model-data discrepancy for each simulation is nega-

tive, indicating our simulations are on average too cool (Table 1). The locations of model-data discrepancies are generally consistent between simulations though vary in magnitude. Temperatures from P-MIO are consistent with or cooler than proxy data, except in NW Bulgaria, the Pannonian Basin, and Shanwang (China) (Table 1). Mean model-data discrepancy for P-MIO is -0.5 °C. T-MIO is cooler than or consistent with proxies at most locations, but is warmer at Kangaroo Well (Australia), Potosi (Bolivia), and the Yunnan Province (China). Mean model-data discrepancy for T-MIO is -1.1 °C. W-MIO is cooler than or consistent with proxy data at all locations except NW Bulgaria, the Pannonian Basin, Potosi (Bolivia), and the Yunnan Province (China). Mean model-data discrepancy for W-MIO is -0.4 °C. Thus, globally, W-MIO produces temperatures most consistent with the proxy record (Fig. 6).

Proxy data are concentrated mostly in Europe. Of the 13 proxy locations in this region, T-MIO shows the least agreement, differing to proxy data at eight locations and having a mean model-data discrepancy of -1 °C. P-MIO and W-MIO differ to proxy data at two and three locations, and have mean model-data discrepancies of -0.3 and -0.1 °C, respectively.

Data are sparsely located throughout the rest of the world. Of four proxy temperatures reported for Australia (three of which originate from SE Australia) one is consistently warmer than all three simulations (Sluiter et al., 1995) (Table 1). P-MIO shows the greatest agreement with proxy data from Australia, with a mean model-data discrepancy of -0.9 °C. T-MIO and

W-MIO have mean model-data discrepancies of -1.2 and -1.0 °C, respectively.

Data from Asia are derived from three locations. W-MIO shows the greatest agreement with proxy data from Asia, having a mean model-data discrepancy of -0.8 °C. P-MIO and T-MIO have mean discrepancies of -1.9 and -1.1 °C, respectively. Namling Basin (Tibet) exhibits the largest model-data discrepancy in this study; as great as -8.1 °C in P-MIO (Table 1). However, this site has one of the largest topographic uncertainties, which when applied reduces model-data discrepancy for P-MIO to -0.8 °C. Discrepancies at Namling Basin are significantly lower in T-MIO and W-MIO (-4.3 and -4.5 °C, respectively). The latitude of the Namling Basin is approximately that at which SSTs increase equatorward in T-MIO and W-MIO, compared with P-MIO (Fig. 1).

Data from North America originate from coastal locations at latitudes greater than 40° N. P-MIO shows the greatest agreement with this data, having a mean model-data discrepancy of -0.4 °C, despite featuring identical extratropical SSTs to W-MIO. Model-data discrepancies from North America are up to 1.0 °C greater in W-MIO than P-MIO.

The only proxy temperature close to the equator is from Fejej (Ethiopia) and is underestimated by more than 2 °C in P-MIO. Temperatures in W-MIO and T-MIO show closer agreement.

Mean Annual Precipitation

Not all locations yielding temperature data provide estimates of precipitation (Table 2).

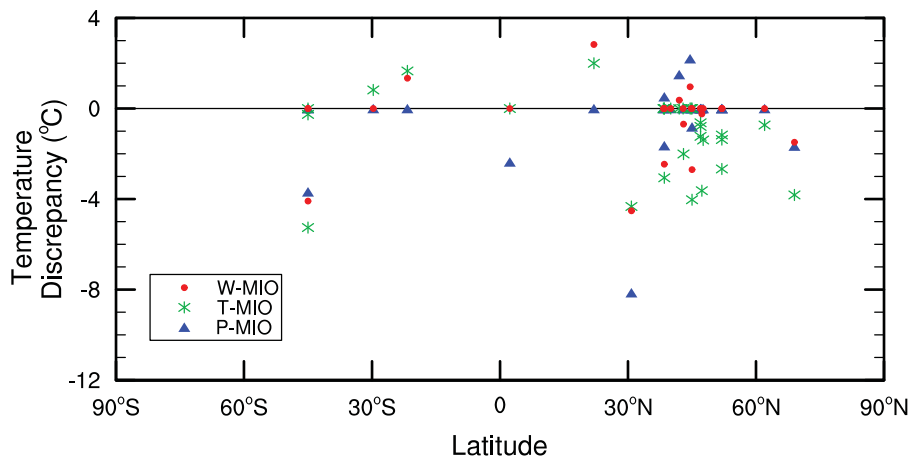


Figure 6. Model-data discrepancies for mean annual 2 m air temperature, plotted as a function of latitude. Refer to Table 1 for values.

Each simulation calculates mean annual precipitation consistent with or lower than the proxy data, except P-MIO, which overestimates precipitation at the Yunnan Province (China) (Fig. 7). On average all three simulations significantly underestimate precipitation. T-MIO underestimates precipitation by an average of -130 mm/yr, though it provides the closest match with proxy data. W-MIO and P-MIO underestimate precipitation by an average of -170 and -320 mm/yr, respectively. Locations of model-data discrepancies are comparable across simulations (Table 2).

DISCUSSION

Mean annual 2 m air temperature is on average underestimated in all three simulations. W-MIO, our “warmest” simulation, provides the closest agreement with proxy data, while

T-MIO shows the least agreement (Table 1). This is attributed to the steeper meridional SST gradient in T-MIO (Fig. 1) and the concentration of proxy data at middle to high latitudes (Fig. 6). Several middle to high latitude locations experience cooler temperatures in W-MIO compared with P-MIO (Fig. 6), despite the two simulations having identical extra-tropical SSTs. The lower temperatures at these locations are part of a broad cooling in W-MIO of up to 4 °C, relative to P-MIO, across parts of middle to high latitude Eurasia and North America (not shown). This cooling is manifest at the 850 and 500 mb pressure levels and is associated with a slightly more pronounced ridge and trough system in the upper atmosphere. This has previously been noted in response to steepening of the meridional temperature gradient (Rind, 2000).

Mean annual precipitation is significantly underestimated in each simulation, though

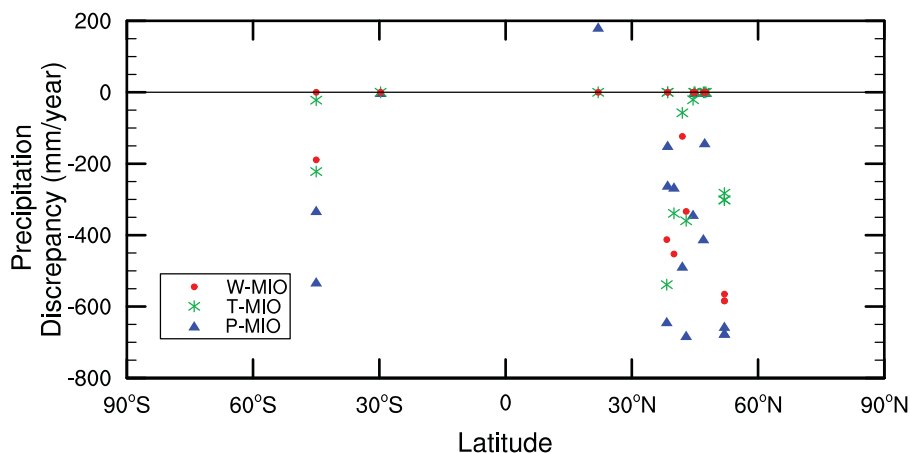


Figure 7. Model-data discrepancies for mean annual precipitation, plotted as a function of latitude. Refer to Table 2 for values.

T-MIO is most consistent with proxy data (Table 2). An increase in tropical SSTs of ~ 4 °C between P-MIO and W-MIO (Fig. 1) reduces the mean model-data discrepancy from -320 to -170 mm/yr. Given that most proxy locations reside in the extra-tropics, this supports tropical SSTs as being the primary driver of global precipitation (Rind, 2000). Cool tropical SSTs may therefore contribute to the significant precipitation discrepancies experienced in all three simulations, particularly P-MIO. The east-west gradient of sea-surface temperatures are also not representative of Miocene conditions and given the proximity of the proxy data to the ocean may have a considerable affect on model-data comparisons. However, simulated temperatures in W-MIO, our “warmest” simulation, show good agreement with proxy data and hence increasing tropical SSTs would likely decrease model-data agreement in this regard (Fig. 6).

Sources of Uncertainty

Model-data discrepancies in this study can be attributed to error in (1) the proxy record, (2) model boundary conditions, and/or (3) model bias. The majority of proxy data used in this study is based upon assumptions of evolution or physiognomic correlation with the environment. The coexistence approach (Mosbrugger and Utescher, 1997) presumes the nearest living relatives of a number of fossil flora at a single location have overlapping environmental tolerances (such as for mean annual temperature and precipitation). This overlap is used to define the paleo-environment of the fossil flora. A shortcoming of this method is that inherent taxonomical differences between fossil and extant floras ensure a decreasing accuracy with increasing age (Uhl et al., 2003). Errors in the identification of fossils can also lead to inaccurate results and many taxonomic data are continuously revised (Uhl et al., 2003), thus actual discrepancies between our model results and the paleo-environment are potentially more or less accurate than indicated here.

Methods of leaf margin analysis, such as the Climate Leaf Analysis Multivariate Program (Wolfe, 1993), correlate present-day leaf characteristics and climate data to fossil leaves to reconstruct the paleo-environment. Therefore the reconstructed climate is not a function of taxonomy. However, since relatively complete leaf margins are required, this method is limited to areas of high sedimentation and precludes the use of microfossils. This highlights a bias of all fossil flora records toward sediment rich areas such as lakes and wetlands. Consequently, reconstructions of climate based on fossil flora alone are potentially wetter and

warmer than the large-scale environments they are used to represent.

A significant proportion of model-data discrepancies may be attributed to smoothed topography in our model. This is exemplified by the Namling Basin, where the model-data discrepancy is eliminated or significantly reduced in each simulation with the application of topographic error (Table 1). We note modern-day simulations with CAM and CLM overestimate snowfall and underestimate temperature over Tibet (Dickinson et al., 2006), suggesting simulated temperatures at Namling Basin would be too cool even at correct elevation. Mean model-data discrepancy for each simulation is reduced by more than half when topographic uncertainty is considered (Table 1). However, this is not an ideal measure of model accuracy given that the calculated topographic errors represent extreme cases and may in fact overestimate topographic uncertainties for the Miocene, and that the degree of overlap between model and proxy temperatures is not considered. As methods of quantifiable error prediction develop for various means of climatic reconstruction, more attention needs to focus on how they can be integrated into model-data comparisons.

Unquantifiable uncertainties in our boundary conditions also need to be considered. In excluding a dynamic ocean model we preclude the oceans response to atmospheric forcing, in other words atmosphere and continental temperatures can evolve during a simulation while SSTs cannot. The global mean residual energy flux at the top level of CAM for P-MIO, T-MIO, and W-MIO is 7.8, 0.08, and 0.3 W/m², respectively. In a dynamic ocean model significant SST responses to the prescribed boundary conditions might be expected. While T-MIO and W-MIO are close to a radiative equilibrium, redistribution of heat in the oceans would likely occur, particularly due to differences in Miocene geography such as closure of the Bering Strait, opening of the Isthmus of Panama, and widening of the Indonesian Throughflow. The Bering Strait is responsible for freshening North Atlantic waters via North Pacific flow through the Arctic, and its closure has been demonstrated to increase North Atlantic salinity and overturning, resulting in warmer SSTs (Wadley and Bigg, 2002). Coupled models demonstrate that North Atlantic overturning decreases and SSTs cool when the Panama Seaway is open (Lunt et al., 2008b). Additionally, the Indonesian Throughflow was dominated by relatively warm South Pacific waters prior to 4 Ma, due to the southward location of the Australian continental plate (Cane and Molnar, 2001). Thus our comparisons with proxy data from areas around the Arctic and North Pacific, as well as

in Europe, are likely to be the most affected by the fixing of SSTs.

Bias in CAM and CLM has been discussed in detail previously (Collins et al., 2006; Dickinson et al., 2006). Of relevance to our simulations are large biases over areas where proxy data exist. Surprisingly, CLM overestimates winter 2 m air temperature by up to 10 °C in the present-day high latitudes of North America and Siberia, enough to significantly affect mean annual values (Dickinson et al., 2006). Thus our model-data discrepancies at Alaska and Cook Inlet could be considered conservative (Table 1). This is largely attributed to excessive low cloud production and downward long wave radiation in CAM (Dickinson et al., 2006). Conversely, simulated temperatures over the Tibetan Plateau are underestimated; for at least half of the year 2 m air temperature is ~5 °C cooler than modern day observations, due to excessive low cloud production and snowfall (Dickinson et al., 2006). Combined with large topographic uncertainty for the Tibetan Plateau (Table 1), modeled temperatures are potentially more than 10 °C too cool. A caveat to these biases is the inherent modifications required for paleoclimate simulations, such as to aerosols, chlorofluorocarbons, greenhouse gases, geography, vegetation, and soil parameters, therefore these discrepancies serve only as a qualitative assessment of model bias.

Comparison with Other Studies of Miocene Climate

In this section we consider our results in the context of recent Miocene modeling studies. In an instructive examination of proxy data acquisition Lunt et al. (2008a) conduct seven simulations of late Miocene climate using differing SST distributions. Despite the abrupt cooling separating the early middle and late Miocene (Lear et al., 2000), broad comparisons can be made with our experiments. Lunt et al. (2008a) use the HadAM3, which runs at a similar resolution to CAM and CLM, as well as an adjusted Miocene topography, which, with the exception of Tibetan Plateau elevation, is similar to ours on the scale of global climate. The authors preclude a late Miocene vegetation profile, opting to prescribe globally homogenous vegetation based on mean values of modern-day vegetation and soil parameters. Vegetation is an important boundary condition for simulating Miocene terrestrial climate (Micheels et al., 2007) and reducing the meridional temperature gradient (Dutton and Barron, 1997). However, the most fundamental difference between this study and Lunt et al. (2008a) is the SST distributions tested. Lunt et al. (2008a) derive a function which varies preindustrial SST with regard to mean global

warming, meridional temperature gradient, and seasonality, while this study tests idealized variations to a proxy derived meridional temperature gradient. Consequently, SST gradients in Lunt et al. (2008a) are steeper than in this study. Lunt et al. (2008a) compare mean values of their model output to midpoints of compiled proxy data and therefore do not take climatic variability into account. To draw comparison with their study, we use the same method here and calculate absolute mean model-data temperature discrepancies for P-MIO, T-MIO, and W-MIO of 2.2, 3.5, and 2.4 °C, respectively. Lunt et al. (2008a) calculate absolute mean model-data discrepancies ranging from 3 to 6.2 °C for their seven simulations.

As noted in our results, CAM and CLM considerably underpredict mean annual precipitation compared to proxy data. Using the same method as Lunt et al. (2008a) we calculate absolute mean model-data discrepancies for P-MIO, T-MIO, and W-MIO of 730, 400, and 460 mm/yr, respectively. Discrepancies in Lunt et al. (2008a) range from 310 to 385 mm/yr. Therefore, performance of CAM and CLM is on par with HadAM3 when calculating temperature; however, they significantly underperform with regard to precipitation.

Micheels et al. (2007) conduct a late Miocene simulation using the ECHAM4 model. Their model setup is similar to ours with the exception that the authors use a mixed layer ocean model (i.e., they do not prescribe SSTs) forced with an adjusted Miocene heat flux. The ECHAM4 is run at a similar resolution to CAM and CLM and includes a Miocene topography and vegetation. The present study uses the same method of model-data comparison as Micheels et al. (2007), therefore results are directly comparable. Micheels et al. (2007) calculate a mean model-data discrepancy for temperature and precipitation of -2.4 °C and -42 mm/yr, respectively. Similar to our comparison with Lunt et al. (2008a), our simulations perform well with respect to temperature prediction, however, significantly underestimate precipitation (Tables 1 and 2).

Subtleties between the models and model setup used in Lunt et al. (2008a), Micheels et al. (2007), and this study do not allow a detailed comparison of results. Particularly, proxy data for the late Miocene generally indicate more arid conditions than those for the early to middle Miocene (c.f. Table 2 and Micheels et al., 2007). However, it is clear that improvements in CAM and CLM are required in order to estimate precipitation more consistent with proxy data. While the large precipitation discrepancies in Table 2 may also be an artifact of our chosen SSTs, which do not respond to atmospheric forcing, similar large discrepancies (on the order

of several hundred mm/yr) have been noted in modern-day simulations compared to observations (Dickinson et al., 2006; Hack et al., 2006).

CONCLUSIONS

We conduct three simulations of late-early to early-middle Miocene climate forced with different meridional SST gradients. In order to evaluate the performance of each simulation we draw quantitative comparisons with terrestrial proxy data. The general trend of our simulations is that they underestimate temperature and precipitation (to varying extents).

Precipitation discrepancies are significantly negative in all three simulations. While proxy data may be representative of local environments which experienced greater precipitation than the grid cells they represent in our simulations, other studies of Miocene climate do not exhibit the same magnitude of discrepancies. Furthermore, the prescribed meridional SST gradient in W-MIO, our “warmest” simulation, provides good agreement with temperature proxies, thus it is probable that a significant portion of the precipitation discrepancies can be attributed to model bias or some crucial ocean-atmosphere interaction.

Some portion of the temperature discrepancies is attributable to the inconsistent spatial scales between the proxy data and model grid (Table 1). Nonetheless, given the uncertainties associated with the proxy data, their uneven distribution as a function of latitude, and the reduction in model-data precipitation discrepancies when tropical SSTs are increased, it is unlikely that tropical SSTs similar to those indicated by $\delta^{18}\text{O}$ data (Fig. 1) existed in the Miocene, and were instead likely to be very close to modern-day values. In order to better constrain SST estimates, more marine and terrestrial data are required, particularly from low latitude locations. Implementation of a coupled ocean model may also resolve the extent to which model-data precipitation discrepancies are caused by prescribing SSTs.

ACKNOWLEDGMENTS

This work was carried out using the Australian Centre for Advanced Computing and Communications cluster. We would like to thank Christine Shields, Samuel Levis, and Richard Neale (NCAR) for help with model setup and Matthew Huber for helpful discussions.

REFERENCES CITED

- Akgun, F., Kayseri, M.S. and Akkiraz, M.S., 2007, Palaeoclimatic evolution and vegetational changes during the Late Oligocene-Miocene period in Western and Central Anatolia (Turkey): Palaeogeography, Palaeoclimatology, Palaeoecology, v. 253, p. 56–106.
- Berner, R.A., and Kothavala, Z., 2001, Geocarb III: A Revised Model of Atmospheric CO_2 over Phanerozoic Time: American Journal of Science, v. 301, no. 2, p. 182–204, doi: 10.2475/ajs.301.2.182.
- Bialkowski, A., Châteaufort, J.-J., Cojan, I. and Bauer, H., 2006, Integrated stratigraphy and paleoenvironmental reconstruction of the Miocene series of the Châteaufort Dome, S.E. France: *Eclogae Geologicae Helveticae*, v. 99, no. 1, p. 1–15.
- Bohme, M., Bruch, A.A. and Selmeier, A., 2007, The reconstruction of Early and Middle Miocene climate and vegetation in Southern Germany as determined from the fossil wood flora: Palaeogeography, Palaeoclimatology, Palaeoecology, v. 253, p. 107–130.
- Bonan, G.B., Levis, S., Kergoat, L., and Oleson, K.W., 2002, Landscapes as patches of plant functional types: An integrating concept for climate and ecosystem models: Global Biogeochemical Cycles, v. 16, no. 2, doi: 10.1029/2000GB001360.
- Cane, M.A., and Molnar, P., 2001, Closing of the Indonesian seaway as a precursor to east African aridification around 3–4 million years ago: Nature, v. 411, no. 6834, p. 157–162, doi: 10.1038/35075500.
- Cerling, T.E., 1991, Carbon dioxide in the atmosphere; evidence from Cenozoic and Mesozoic Paleosols: American Journal of Science, v. 291, no. 4, p. 377–400.
- Christophel, D.C. and Greenwood, D.R., 1989, Changes in climate and vegetation in Australia during the tertiary: Review of Palaeobotany and Palynology, v. 58, p. 95–109.
- Collins, W.D., Rasch, P.J., Boville, B.A., Hack, J.J., McCaa, J.R., Williamson, D.L., Briegleb, B.P., Bitz, C.M., Lin, S.-J., and Zhang, M., 2006, The Formulation and Atmospheric Simulation of the Community Atmosphere Model Version 3 (CAM3): Journal of Climate, v. 19, no. 11, p. 2144–2161, doi: 10.1175/JCLI3760.1.
- Crowley, T.J., and Zachos, J.C., 2000, Comparison of zonal temperature profiles for past warm time periods, in Huber, B.T., MacLeod, K.G., and Wing, S.L., eds., Warm climates in Earth history: Cambridge, University of Cambridge, p. 50–76.
- Devereux, I., 1967, Oxygen isotope paleotemperature measurements on New Zealand Tertiary fossils: New Zealand Journal of Science, v. 10, no. 4, p. 988–1011.
- Dickinson, R.E., et al., 2006, The Community Land Model and its climate statistics as a component of the Community Climate System Model: Journal of Climate, v. 19, no. 11, p. 2302–2324, doi: 10.1175/JCLI3742.1.
- Ducrocq, S., Chaimanee, Y., Suteethorn, V. and Jaeger, J.J., 1994, Ages and palaeoenvironment of Miocene mammalian faunas from Thailand: Palaeogeography, Palaeoclimatology, Palaeoecology, v. 108, p. 149–163.
- Dutton, J.F., and Barron, E.J., 1997, Miocene to present vegetation changes: a possible piece of the Cenozoic cooling puzzle: Geology, v. 25, no. 1, p. 39–41, doi: 10.1130/0091-7613(1997)025<0039:MTPVCA>2.3.CO;2.
- Erdei, B., Hably, L., Kazmer, M., Utescher, T. and Bruch, A.A., 2007, Neogene flora and vegetation development of the Pannonian domain in relation to palaeoclimate and palaeogeography: Palaeogeography, Palaeoclimatology, Palaeoecology, v. 253, p. 131–156.
- Francois, L., Grad, A., and Godderis, Y., 2005, Modelling atmospheric CO_2 changes at geological time scales: Carnets de Géologie, v. M02, p. 11–14.
- Graham, A., 1987, Miocene Communities and Palaeoenvironments of Southern Costa Rica: American Journal of Botany, v. 74, p. 1501–1518.
- Greenwood, D.R., 1994, Palaeobotanical evidence for Tertiary climates, in Hill, R.S., ed., The History of Australian Vegetation: Cretaceous to Recent: Cambridge, Cambridge University Press, p. 44–59.
- Gregory-Wodzicki, K.M., McIntosh, W.C. and Velasquez, K., 1998, Climatic and tectonic implications of the late Miocene Jakokkota flora, Bolivian Altiplano: Journal of South American Earth Sciences, v. 11, p. 533–560.
- Hack, J.J., et al., 2006, Simulation of the global hydrological cycle in the CCSM Community Atmosphere Model version 3 (CAM3): Mean features: Journal of Climate, v. 19, no. 11, p. 2199–2221, doi: 10.1175/JCLI3755.1.
- Harris, N., 2006, The elevation history of the Tibetan Plateau and its implications for the Asian monsoon: Palaeogeography, Palaeoclimatology, Palaeoecology, v. 241, no. 1, p. 4–15, doi: 10.1016/j.palaeo.2006.07.009.
- Herold, N., Seton, M., Müller, R.D., You, Y., and Huber, M., 2008, Middle Miocene tectonic boundary conditions for use in climate models: Geochemistry Geophysics Geosystems, v. 9, p. Q10009.
- Huber, M., and Sloan, L.C., 2000, Climatic responses to tropical sea surface temperature changes on a “greenhouse”: Earth: Paleoclimatology, v. 15, no. 4, p. 443–450, doi: 10.1029/1999PA000455.
- Huber, M., and Sloan, L.C., 2001, Heat transport, deep waters, and thermal gradients: Coupled simulation of an Eocene greenhouse climate: Geophysical Research Letters, v. 28, no. 18, p. 3481–3484, doi: 10.1029/2001GL012943.
- Ivanov, D., Ashraf, A.R., Mosbrugger, V. and Palamarev, E., 2002, Palynological evidence for Miocene climate change in the Forecarpathian Basin (Central Paratethys, NW Bulgaria): Palaeogeography, Palaeoclimatology, Palaeoecology, v. 178, p. 19–37.
- Jacobs, B.F., 2004, Palaeobotanical studies from tropical Africa: Relevance to the evolution of forest, woodland and savannah biomes: Philosophical Transactions of the Royal Society of London Series B Biological Sciences, v. 359, p. 1573–1583.
- Kemp, E.M., 1978, Tertiary climatic evolution and vegetation history in the Southeast Indian Ocean region: Palaeogeography, Palaeoclimatology, Palaeoecology, v. 24, p. 169–208.
- Kennett, J.P., Keller, G., and Srinivasan, M.S., 1985, Miocene planktonic foraminiferal biogeography and paleoceanographic development of the Indo-Pacific region: Memoir: Geological Society of America, v. 163, p. 197–236.
- Kiehl, J.T., and Shields, C.A., 2005, Climate simulation of the latest Permian: Implications for mass extinction: Geology, v. 33, no. 9, p. 757–760, doi: 10.1130/G21654.1.
- Kürschner, W.M., Kvacek, Z., and Dilcher, D.L., 2008, The impact of Miocene atmospheric carbon dioxide fluctuations on climate and the evolution of terrestrial ecosystems: Proceedings of the National Academy of Sciences of the United States of America, v. 105, no. 2, p. 449–453, doi: 10.1073/pnas.0708588105.
- Lear, C.H., Elderfield, H., and Wilson, P.A., 2000, Cenozoic deep-sea temperatures and global ice volumes from Mg/Ca in benthic foraminiferal calcite: Science, v. 287, no. 5451, p. 269–272, doi: 10.1126/science.287.5451.269.
- Liang, M.-M., Bruch, A., Collinson, M., Mosbrugger, V., Li, C.-S., Sun, Q.-G., and Hilton, J., 2003, Testing the climatic estimates from different palaeobotanical methods: An example from the Middle Miocene Shanwang flora of China: Palaeogeography, Palaeoclimatology, Palaeoecology, v. 198, 279–301.
- Lunt, D.J., et al., 2008a, A methodology for targeting palaeo proxy data acquisition: A case study for the terrestrial late Miocene: Earth and Planetary Science Letters, v. 271, no. 1–4, p. 53–62, doi: 10.1016/j.epsl.2008.03.035.
- Lunt, D.J., Valdes, P.J., Haywood, A., and Rutt, I.C., 2008b, Closure of the Panama Seaway during the Pliocene: Implications for climate and Northern Hemisphere glaciation: Climate Dynamics, v. 30, no. 1, p. 1–18, doi: 10.1007/s00382-007-0265-6.
- Martin, H.A., 1990, Tertiary climate and phytogeography in southeastern Australia: Review of Palaeobotany and Palynology, v. 65, p. 47–55.
- Martin, H.A., 2006, Cenozoic climatic change and the development of the arid vegetation in Australia: Journal of Arid Environments, v. 66, p. 533–563.
- Megirian, D., Murray, P., Schwartz, L. and Von Der Borch, C., 2004, Late Oligocene Kangaroo Well Local Fauna from the Ula Limestone (new name), and climate of the Miocene oscillation across central Australia: Australian Journal of Earth Sciences, v. 51, p. 701–741.
- Micheels, A., Bruch, A.A., Uhl, D., Utescher, T., and Mosbrugger, V., 2007, A Late Miocene climate model simulation with ECHAM4/ML and its quantitative validation with terrestrial proxy data: Palaeogeography, Palaeoclimatology, Palaeoecology, v. 253, no. 1–2, p. 251–270, doi: 10.1016/j.palaeo.2007.03.042.
- Mildenhall, D.C., 1980, New Zealand late Cretaceous and Cenozoic plant biogeography: A contribution: Palaeogeography, Palaeoclimatology, Palaeoecology, v. 31, p. 197–233.
- Mosbrugger, V., and Utescher, T., 1997, The coexistence approach—A method for quantitative reconstructions

- of Tertiary terrestrial palaeoclimate data using plant fossils: *Palaeogeography, Palaeoclimatology, Palaeoecology*, v. 134, no. 1–4, p. 61–86, doi: 10.1016/S0031-0182(96)00154-X.
- Mosbrugger, V., Utescher, T. and Dilcher, D.L., 2005. Cenozoic continental climatic evolution of Central Europe: *PNAS*, v. 102, no. 42, p. 14964–14969.
- Müller, R.D., Sdrolias, M., Gaina, C. and Roest, W.R., 2008. Age, spreading rates, and spreading asymmetry of the world's ocean crust: *Geochem. Geophys. Geosyst.*, v. 9, p. Q04006.
- O'Connell, S., Chandler, M.A., and Ruedy, R., 1996. Implications for the creation of warm saline deep water; late Paleocene reconstructions and global climate model simulations: *Geological Society of America Bulletin*, v. 108, no. 3, p. 270–284, doi: 10.1130/0016-7606(1996)108<0270:IFTCOW>2.3.CO;2.
- Pagani, M., Arthur, M.A., and Freeman, K.H., 1999a. Miocene evolution of atmospheric carbon dioxide: *Paleoceanography*, v. 14, no. 3, p. 273–292, doi: 10.1029/1999PA900006.
- Pagani, M., Freeman, K.H., and Arthur, M.A., 1999b. Late Miocene atmospheric CO₂ concentrations and the expansion of C₄ grasses: *Science*, v. 285, no. 5429, p. 876–879, doi: 10.1126/science.285.5429.876.
- Pearson, P.N., et al., 2001. Warm tropical sea surface temperatures in the Late Cretaceous and Eocene epochs: *Nature*, v. 413, no. 6855, p. 481–487, doi: 10.1038/35097000.
- Pearson, P.N., and Palmer, M.R., 2000. Atmospheric carbon dioxide concentrations over the past 60 million years: *Nature*, v. 406, no. 6797, p. 695–699, doi: 10.1038/35021000.
- Pearson, P.N., et al., 2007. Stable warm tropical climate through the Eocene Epoch: *Geology*, v. 35, no. 3, p. 211–214, doi: 10.1130/G23175A.1.
- Pekar, S.F., and DeConto, R.M., 2006. High-resolution ice-volume estimates for the early Miocene: Evidence for a dynamic ice sheet in Antarctica: *Palaeogeography, Palaeoclimatology, Palaeoecology*, v. 231, no. 1–2, p. 101–109, doi: 10.1016/j.palaeo.2005.07.027.
- Retallack, G.J., 2001. A 300-million-year record of atmospheric carbon dioxide from fossil plant cuticles: *Nature*, v. 411, no. 6835, p. 287–290, doi: 10.1038/35077041.
- Retallack, G.J., 2004. Late Miocene climate and life on land in Oregon within a context of Neogene global change: *Palaeogeography, Palaeoclimatology, Palaeoecology*, v. 214, p. 97–123.
- Rind, D., 2000. Relating paleoclimate data and past temperature gradients: Some suggestive rules: *Quaternary Science Reviews*, v. 19, no. 1–5, p. 381–390.
- Royer, D.L., et al., 2001. Paleobotanical evidence for near present-day levels of atmospheric CO₂ during part of the Tertiary: *Science*, v. 292, no. 5525, p. 2310–2313, doi: 10.1126/science.292.5525.2310.
- Savin, S.M., Douglas, R.G., and Stehli, F.G., 1975. Tertiary marine paleotemperatures: *Geological Society of America Bulletin*, v. 86, p. 1499–1510.
- Shackleton, N.J., and Kennett, J.P., 1975. Paleotemperature history of the Cenozoic and the initiation of Antarctic glaciation: oxygen and carbon isotope analyses in DSDP sites 277, 279, and 281: *Initial Reports of the Deep Sea Drilling Project*, v. 29, p. 743–755.
- Sheldon, N.D., 2006. Using paleosols of the Picture Gorge Basalt to reconstruct the middle Miocene climatic optimum: *PaleoBios*, v. 26, no. 2, p. 27–36.
- Shevenell, A.E., Kennett, J.P., and Lea, D.W., 2004. Middle Miocene Southern Ocean Cooling and Antarctic Cryosphere Expansion: *Science*, v. 305, no. 5691, p. 1766–1770, doi: 10.1126/science.1100061.
- Sloan, L.C., and Barron, E.J., 1992. A comparison of Eocene climate model results to quantified paleoclimatic interpretations: *Palaeogeography, Palaeoclimatology, Palaeoecology*, v. 93, no. 3–4, p. 183–202, doi: 10.1016/0031-0182(92)90096-N.
- Sloan, L.C., Huber, M., Crowley, T.J., Sewall, J.O., and Baum, S., 2001. Effect of sea surface temperature configuration on model simulations of “equable” climate in the Early Eocene: *Palaeogeography, Palaeoclimatology, Palaeoecology*, v. 167, no. 3–4, p. 321–335, doi: 10.1016/S0031-0182(00)00245-5.
- Sloan, L.C., and Rea, D.K., 1996. Atmospheric carbon dioxide and early Eocene climate: A general circulation modeling sensitivity study: *Palaeogeography, Palaeoclimatology, Palaeoecology*, v. 119, no. 3–4, p. 275–292, doi: 10.1016/0031-0182(95)00012-7.
- Sloan, L.C., and Thomas, E., 1998. Global climate of the late Paleocene epoch; modeling the circumstances associated with a climatic “event,” *in* Aubry, M.-P., Lucas, S.G., and Berggren, W.A., eds., *Late Paleocene-early Eocene climatic and biotic events in the marine and terrestrial records*: New York, Columbia University Press, p. 138–157.
- Sluiter, I.R.K., Kershaw, A.P., Holdgate, G.R., and Bulman, D., 1995. Biogeographic, ecological and stratigraphic relationships of the Miocene brown coal floras, Latrobe Valley, Victoria, Australia: *International Journal of Coal Geology*, v. 28, no. 2–4, p. 277–302, doi: 10.1016/0166-5162(95)00021-6.
- Spicer, R.A. et al., 2003. Constant elevation of southern Tibet over the past 15 million years: *Nature*, v. 421, p. 622–624.
- Steppuhn, A., et al., 2007. The sensitivity of ECHAM4/ML to a double CO₂ scenario for the Late Miocene and the comparison to terrestrial proxy data: *Global and Planetary Change*, v. 57, no. 3–4, p. 189–212, doi: 10.1016/j.gloplacha.2006.09.003.
- Stewart, D.R.M., Pearson, P.N., Ditchfield, P.W., and Singano, J.M., 2004. Miocene tropical Indian Ocean temperatures: Evidence from three exceptionally preserved foraminiferal assemblages from Tanzania: *Journal of African Earth Sciences*, v. 40, no. 3–4, p. 173–189, doi: 10.1016/j.jafrearsci.2004.09.001.
- Sun, Q.-G., Collinson, M.E., Li, C.-S., Wang, Y.-F. and Beerling, D.J., 2002. Quantitative reconstruction of palaeoclimate from the Middle Miocene Shanwang flora, eastern China: *Palaeogeography, Palaeoclimatology, Palaeoecology*, v. 180, p. 315–329.
- Syabryaj, S., Utescher, T., Molchanoff, S. and Bruch, A.A., 2007. Vegetation and palaeoclimate in the Miocene of Ukraine: *Palaeogeography, Palaeoclimatology, Palaeoecology*, v. 253, p. 169–184.
- Sykes, T.J.S., Ramsay, A.T.S., and Kidd, R.B., 1998. Southern hemisphere Miocene bottom-water circulation: A palaeobathymetric analysis: *Geological Society [London] Special Publications*, 131, no. 1, p. 43–54.
- Uhl, D., Mosbrugger, V., Bruch, A., and Utescher, T., 2003. Reconstructing palaeotemperatures using leaf floras—Case studies for a comparison of leaf margin analysis and the coexistence approach: *Review of Palaeobotany and Palynology*, v. 126, no. 1–2, p. 49–64, doi: 10.1016/S0034-6667(03)00058-7.
- Uhl, D., Bruch, A.A., Traiser, C. and Klotz, S., 2006. Palaeoclimate estimates for the Middle Miocene Schrotzburg flora (S Germany): A multi-method approach: *International Journal of Earth Sciences*, v. 95, p. 1071–1085.
- Uhl, D., Klotz, S., Traiser, C., Thiel, C., Utescher, T., Kowalski, E., and Dilcher, D.L., 2007. Cenozoic paleotemperatures and leaf physiognomy—A European perspective: *Palaeogeography, Palaeoclimatology, Palaeoecology*, v. 248, p. 24–31.
- Utescher, T., Mosbrugger, V., and Ashraf, A.R., 2000. Terrestrial Climate Evolution in Northwest Germany Over the Last 25 Million Years: *Palaios*, v. 15, p. 430–449.
- Utescher, T., Djordjevic-Milutinovic, D., Bruch, A. and Mosbrugger, V., 2007. Palaeoclimate and vegetation change in Serbia during the last 30 Ma: *Palaeogeography, Palaeoclimatology, Palaeoecology*, v. 253, p. 157–168.
- van der Smidt, J.H., et al., 1996. Organofacies variations in sediments from the continental slope and rise of the New Jersey continental margin (Sites 903 and 905): *Proceedings of the Ocean Drilling Program, Scientific results*, v. 150, p. 329–344.
- Vertenstein, M., Oleson, K., Levis, S., and Hoffman, F., 2004. *Community Land Model Version 3.0 (CLM3.0) User's Guide*, National Center for Atmospheric Research, Boulder.
- von der Heydt, A., and Dijkstra, H.A., 2006. Effect of ocean gateways on the global ocean circulation in the late Oligocene and early Miocene: *Paleoceanography*, v. 21, no. 1, p. PA1011, doi: 10.1029/2005PA001149.
- Wadley, M.R., and Bigg, G.R., 2002. Impact of flow through the Canadian Archipelago and Bering Strait on the North Atlantic and Arctic circulation: An ocean modelling study: *Quarterly Journal of the Royal Meteorological Society*, v. 128, no. 585, p. 2187–2203, doi: 10.1256/qj.00.35.
- White, J.M. and Ager, T.A., 1994. Palynology, paleoclimatology and correlation of Middle Miocene beds from Porcupine River (locality 90-1), Alaska: *Quaternary International*, v. 22–23, p. 43–77.
- Wiemann, M.C., Manchester, S.R. and Wheeler, E.A., 1999. Paleotemperature estimation from dicotyledonous wood anatomical characters: *Palaios*, v. 14, p. 459–474.
- Williams, M., et al., 2005. Evaluating the efficacy of planktonic foraminifer calcite δ¹⁸O data for sea surface temperature reconstruction for the Late Miocene: *Geobios*, v. 38, no. 6, p. 843–863, doi: 10.1016/j.geobios.2004.12.001.
- Wolfe, J.A., 1985. Distribution of major vegetational types during the Tertiary: *Geophysical Monograph*, v. 32, p. 357–375.
- Wolfe, J.A., 1993. A method of obtaining climatic parameters from leaf assemblages: *U.S. Geological Survey Bulletin*, v. 2040, p. 71.
- Wolfe, J.A., 1994a. An analysis of Neogene climates in Beringia: *Palaeogeography, Palaeoclimatology, Palaeoecology*, v. 108, p. 207–216.
- Wolfe, J.A., 1994b. Tertiary climatic changes at middle latitudes of western North America: *Palaeogeography, Palaeoclimatology, Palaeoecology*, v. 108, p. 195–205.
- Wright, J.D., and Thunell, R.C., 1988. Neogene Planktonic Foraminiferal Biogeography and Paleoclimatology of the Indian Ocean: *Micropaleontology*, v. 34, no. 3, p. 193–216, doi: 10.2307/1485752.
- Wynn, J.G. and Retallack, G.J., 2001. Paleoenvironmental reconstruction of middle Miocene paleosols bearing *Kenyapithecus* and *Victoriapithecus*, Nyakach formation, southwestern Kenya: *Journal of Human Evolution*, v. 40, p. 263–288.